Spectrochimica Acta Part A: Molecular and Biomolecular Spectroscopy 344 (2026) 126676

Contents lists available at ScienceDirect

Spectrochimica Acta Part A: Molecular and Biomolecular Spectroscopy

journal homepage: www.journals.elsevier.com/spectrochimica-acta-part-a-molecular-and-biomolecular-spectroscopy

Potential application of hyperspectral imaging for monitoring resin cure in composite manufacturing via liquid resin infusion

Xabier Zurutuza Lasa [a,*], Laura Arévalo Díaz [a], Janusz Poplawski [a], Cristian Builes Cárdenas [b], Tania Grandal González [c], Arantzazu Núñez Cascajero [c], Rubén Ruiz Lombera [c], Paula Rodriguez Alonso [b], Mario Román Rodríguez [b], Daniel Maestro-Watson [d], Luka Eciolaza Echeverria [d]

[a] Digitalization Technologies, LORTEK Technological Centre, Basque Research and Technology Alliance (BRTA), Arranomendia Kalea 4A, Ordizia, 20240, Basque Country, Spain
[b] Advanced Composites Technologies, R&D Division, AIMEN Technology Centre, Polígono Industrial de Cataboi, Sector 2, Parcela 3, O Porriño, 36418, Galicia, Spain
[c] Smart Systems & Smart Manufacturing, R&D Division, AIMEN Technology Centre, Polígono Industrial de Cataboi, Sector 2, Parcela 3, O Porriño, 36418, Galicia, Spain
[d] Electronics and Computer Science department, Mondragon Unibertsitatea, Goiru Kalea 2, Mondragón, 20500, Basque Country, Spain

HIGHLIGHTS

- NIR spectra reveal key curing features of Hexcel RTM6-2 epoxy resin.
- HSI tracks spectral evolution during curing in LRI manufacturing.
- SVR and PLS-R link spectral data to curing state from sensors.
- Predicted curing maps show consistent trends across all defined ROIs.

GRAPHICAL ABSTRACT

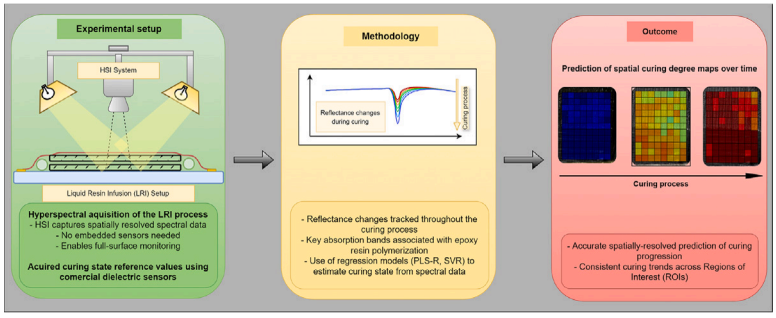

ARTICLE INFO

Dataset link: https://doi.org/10.5281/zenodo.15087655

Keywords:
Near-infrared hyperspectral imaging
Composite manufacturing
Curing state monitoring
Liquid resin infusion
Chemometrics
Machine learning

ABSTRACT

This study investigates the feasibility of using Near-Infrared Hyperspectral Imaging (HSI) for monitoring the curing state in Liquid Resin Infusion (LRI) manufacturing. By capturing spectral reflectance data throughout the heating and curing phases of the process, we explore the potential of HSI as a non-destructive technique for assessing resin polymerization. Compared to conventional sensor-based methods, HSI offers two key advantages: it eliminates the need to embed sensors within the manufactured part and provides spatially resolved information across the entire surface, enabling the detection of cure inhomogeneities. First, an in-depth study was conducted on the spectral features captured by NIR-HSI and their temporal evolution throughout the process, comparing them with key absorption bands related to the epoxy resin used in LRI. Afterwards, spectral data was correlated with the curing state inferred from commercial dielectric sensors using regression models, including Partial Least Squares Regression (PLS-R) and Support Vector Regression (SVR). These regression models were trained using the full spectral range of a specific spatial region of interest, as

* Corresponding author.
E-mail addresses: xzurutuza@lortek.es (X. Zurutuza Lasa), larevalo@lortek.es (L. Arévalo Díaz), jpoplawski@lortek.es (J. Poplawski), cristian.builes@aimen.es (C.B. Cárdenas), tania.grandal@aimen.es (T.G. González), arantzazu.nunez@aimen.es (A.N. Cascajero), ruben.ruiz@aimen.es (R.R. Lombera), paula.rodriguez@aimen.es (P.R. Alonso), mario.roman@aimen.es (M.R. Rodríguez), dmaestro@mondragon.edu (D. Maestro-Watson), leciolaza@mondragon.edu (L.E. Echeverria).

https://doi.org/10.1016/j.saa.2025.126676
Received 31 March 2025; Received in revised form 4 July 2025; Accepted 7 July 2025
Available online 17 July 2025

well as wavelength subsets selected through feature selection techniques such as Mutual Information (MI) and Random Forest Regressor (RF). The results indicate a strong correlation between the spectral data and the inferred curing state, with the SVR model trained on the full spectral range achieving the highest performance ($R^2 = 0.9983$, RMSE = 0.0114, MAE = 0.0086). Moreover, the predicted curing maps display consistent trends across all defined regions of interest (ROIs), further demonstrating the capability of HSI to capture spatial variations in the curing process. These findings reinforce the potential of Near-Infrared Hyperspectral Imaging as a powerful, non-destructive tool for real-time monitoring of resin polymerization in LRI manufacturing.

1. Introduction

Composite materials consist of two or more combined components, offering enhanced performance compared to a single material. Typically, this combination results in greater strength, stiffness and lower density. Based on the interaction between the dispersed component, also called the reinforcement, and the matrix, they fall into three main families: particle-reinforced composites, where uniformly distributed ceramic or metallic particles arrest dislocations and cracks to raise isotropic wear resistance and modulus; fibre-reinforced composites, in which short, long, or continuous fibres (glass, carbon, aramid, etc.) carry most of the load and deliver exceptional directional strength and stiffness; and structural or laminate composites, whose performance stems from stacking or sandwiching layers or low-density cores, yielding high bending stiffness-to-weight and impact tolerance [1,2]. By selecting the right combination of reinforcement and matrix material, the resulting part will meet the specific requirements for a particular application [3]. The unique characteristics of composite materials have led to their increasingly widespread use in the energy, aerospace, naval, and automotive manufacturing sectors, where fibre-reinforced polymers are one of the most attractive materials [4].

Several procedures can be employed to manufacture composite parts. Liquid Composite Moulding (LCM) encompasses a family of processes in which a dry fibrous reinforcement is impregnated with liquid resin inside a sealed cavity [5]. The vacuum infusion process, also called vacuum assisted resin infusion or Liquid Resin Infusion (LRI), is one of the most widely used LCM processes in composite manufacturing, especially for producing large parts like wind turbine rotor blades, aircraft wing covers or ships decks. In all LCM procedures, a multi-layer fibre preform is placed in a mould and infused with liquid resin under vacuum pressure. Once the resin is cured, the finished part is extracted from the mould, resulting in a solid composite structure. LRI has gained significant popularity in recent years due to its ability to produce high-quality complex parts with superior mechanical properties [6]. Key advantages of LRI include lower tooling costs and the capacity to create larger, intricate components, making it particularly appealing for industries such as aerospace and automotive, which require lightweight and durable materials.

In composite manufacturing by LRI, multiple steps must be carefully performed to ensure product quality. Many of these steps present potential defects and require a quality control process. Automating all these steps can enhance process control, increase overall resource efficiency, and promote a more sustainable manufacturing approach. One of the first steps in the manufacturing process is the mould preparation and fibre layup, that must be executed with precision to prevent misalignment and wrinkles, as these can compromise the integrity of the final part. Visual inspection and laser projection systems can be employed to ensure the accurate placement of the fibres [7,8]. During the resin infusion stage, it is essential to monitor the resin flow to avoid dry spots or voids within the composite. Advanced monitoring techniques, such as fibre optic sensors, can be utilized to track the resin distribution in real-time [9], allowing for on-the-fly adjustments to ensure complete impregnation of the fibres.

After infusion, the curing process in the Liquid Resin Infusion (LRI) method must be meticulously controlled to prevent issues such as resin-rich areas or incomplete curing, which can adversely affect the mechanical properties of the composite. An inhomogeneous curing process can lead to increased residual stresses in the manufactured part, significantly impacting material performance [10]. Monitoring the curing stage is therefore critical, as an incomplete or improperly cured component can result in deformation, loss of strength, or other defects that may necessitate costly repairs or even part rejection. To address these challenges, various in situ techniques are employed to assess the degree of cure and ensure process uniformity. Temperature sensors and dielectric analysis (DEA) using Direct Current (DC) provide valuable real-time data during the curing process [11–13], allowing for the detection of deviations and ensuring the process proceeds correctly [14]. DEA, for instance, offers high sensitivity by tracking changes in the resin's dielectric properties — such as permittivity or loss factor — throughout the curing cycle. However, it has limitations including the need for direct contact, potential sensor wear, contamination risks, and complex data interpretation [15]. Its accuracy may also be compromised by process-related factors such as release agents, and it lacks the ability to detect cure inhomogeneities across the part. Temperature sensors, on the other hand, monitor internal thermal evolution and enable estimation of the degree of cure by comparing measured profiles against thermo-kinetic models or simulations of the resin system [16]. These models are typically developed offline using techniques such as Differential Scanning Calorimetry (DSC) or rheometric analysis to characterize the curing kinetics of new materials [17], thus adding a necessary preparatory step. Like dielectric sensors, thermocouples also require embedding within the part, which may pose practical constraints in some applications.

A recently reported promising method for inline monitoring of resin cure degree is Near-Infrared (NIR) spectroscopy [18]. While NIR spectroscopy has been extensively utilized at the laboratory level to assess the chemical parameters of resins [19], recent work proposes its application in industrial environments, accounting for process variability. In this approach, the degree of cure is determined by capturing NIR spectral data of the resin during the curing process, in parallel with reference measurements obtained through differential scanning calorimetry. A Partial Least Squares (PLS) regression model is then developed, achieving high accuracy in predicting the degree of cure. The results of this work have shown that the NIR spectroscopy offers a powerful approach for determining the degree of cure, as it is real-time, non-contact, and non-destructive. However, its main limitation is that it provides measurements at a single point on the sample.

In this study, the primary objective is to evaluate the feasibility of utilizing Near-Infrared Hyperspectral Imaging (NIR-HSI) to track the cure progression during the LRI process. HSI captures the light reflected by the sample and, by acquiring several hyperspectral images over time, generates distinct spectral signatures that can be analysed to identify chemical-composition changes [20]; moreover, such changes can be detected through a multivariable model. The core strength of this technology lies in its ability to simultaneously combine spatial and spectral information within a single measurement, providing a non-destructive approach to characterizing samples based on their spectral signatures across the entire surface. While HSI has demonstrated its potential in various manufacturing domains, such as the pharmaceutical [21,22] and food [23,24] industries, its application in composite material manufacturing remains relatively underexplored [25]. Traditional monitoring methods often rely on point measurements or post-process evaluations, which can miss critical variations throughout

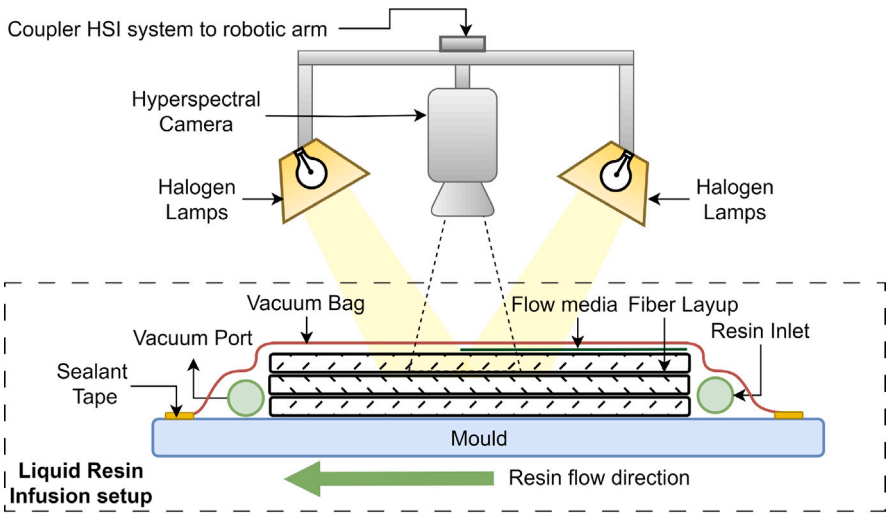

Fig. 1. Diagram of the experimental setup illustrating the LRI process and its inspection using a hyperspectral imaging system.

the curing phase throughout the entire composite part. In contrast, NIR-HSI provides continuous insights into the state of cure across the entire component, enabling early detection of curing anomalies that may affect the final part. In this work, the potential application of an HSI system for monitoring the curing state in a composite manufacturing process is demonstrated for the first time, paving the way for new applications of these systems and offering the composites industry an innovative method for manufacturing process control.

The remainder of this article is structured as follows: Section 2 details the experimental setup and techniques used in this study. It begins with an overview of the LRI process and its materials, followed by a description of the reference measurement methods employed to infer the reference curing state. The section concludes with an explanation of the hyperspectral imaging system, including data acquisition and analysis procedures. Section 3 presents the findings of the study, starting with the spectral characterization of the materials used on LRI, and then discussing hyperspectral images acquired during the LRI process. Finally, Section 4 provides the conclusions drawn from the study, summarizing key insights and future steps.

2. Material and methods

2.1. Liquid resin infusion materials and process description

The LRI process is schematically illustrated in Fig. 1. A dry fibre layup, composed of carbon fibres, is stacked according to the part design within a mould and enclosed in a vacuum-sealed bag. Vacuum pressure is applied through a port, evacuating air and creating a pressure gradient that draws liquid resin from an inlet tube into the fibre preform. To ensure uniform resin distribution and complete impregnation, a flow medium is placed on the uppermost layer of the fibre preform, facilitating enhanced wet-out. Finally, the infused composite is cured under heat (provided by a heating plate) until fully hardened, resulting in the final part. Using this process, two rectangular composite samples (Sample A and Sample B) were produced for the study.

The materials selected for this study comply with the requirements of the aeronautical sector, consisting of carbon fibre and high-performance epoxy resin. Specifically, 4 layers of bidirectional Zoltek Panex 35–13 50K 4 fabrics were arranged in a symmetrical and balanced $[0/90/0/90]_{2s}$ sequence, forming a preform with dimensions of 280×200 mm. The chosen resin was Hexcel HexFlow RTM6-2, a bi-component epoxy resin specifically formulated for high performance applications. This resin requires a specific temperature ramp to ensure proper curing. To facilitate uniform resin flow and impregnation, a polymer flow media was placed over half of the sample, covering the inlet region. Finally, a polymer vacuum bag was employed to maintain vacuum conditions.

Infusion process begins when the preform reaches 100 °C–120 °C to ensure low viscosities for resin infusion (≈100 mPa s). Once the preform reached this temperature, the resin inlet valve is opened to initiate fibre impregnation (infusion stage). After complete impregnation, the inlet channel is closed, and the temperature is increased to 180 °C (heating phase). This temperature is maintained for two hours (curing phase) to fully cure the resin and complete the manufacturing process. This process is normally done inside an oven to ensure controlled and uniform curing conditions. However, in the context of this feasibility study, and due to the temperature constraints of placing the hyperspectral camera inside the oven, LRI process was conducted on a self-heated open mould (by oil circuit). Fig. 2(a) shows the self-heated mould along with the fibre layup. The challenge of camera integration into an oven is beyond the scope of this study but could be explored in future work.

2.2. Reference measurement for curing state estimation

The degree of cure is a dimensionless quantity and key parameter in thermosetting resin systems that describes the extent to which the resin has undergone chemical cross-linking during the curing process. It is typically expressed as a ratio or percentage, where 0% (or 0) corresponds to the uncured state and 100% (or 1) indicates a fully cured resin. While the degree of cure can be directly measured using techniques such as Differential Scanning Calorimetry (DSC), it can also be estimated indirectly from material properties that evolve during curing. In this study, Dielectric Analysis (DEA) was used to infer the curing state through a commercial dielectric sensor. Specifically, the sensor used in this study is a disposable sensor from *Synthesites* [26] acquired with their *Optimold* data acquisition equipment, which is widely recognized for its reliability in composite curing applications using RTM6-2 [27].

The dielectric sensor monitors the resin's molecular mobility through resistance measurements of its sensing element, enable real-time phase detection during LRI process. Two dielectric sensors were positioned at specific monitoring points between the mould and the fabric layers to maintain continuous resin contact throughout curing. One sensor was placed near the resin inlet and the other near the resin outlet port (Fig. 2(b)), obtaining discrete measurements at two separate locations within the sample.

As shown in Fig. 3(a), the response of the sensors enables visualization of both infusion and curing phases. Upon resin contact (impregnation phase), the sensor typically registers values around 50

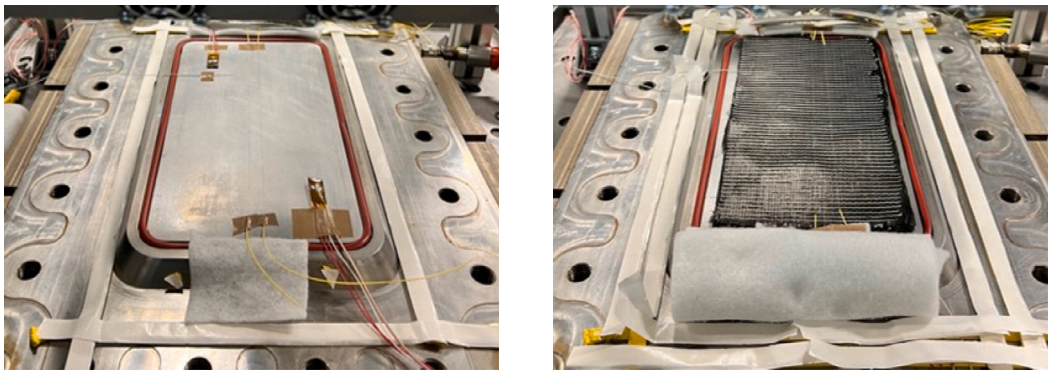

(a) (b)

Fig. 2. (a) Two dielectric sensors placed on top of the self-heated mould, ensuring contact with the fibre preform. (b) Fibre preform placed in the self-heated mould where the LRI process will be carried out.

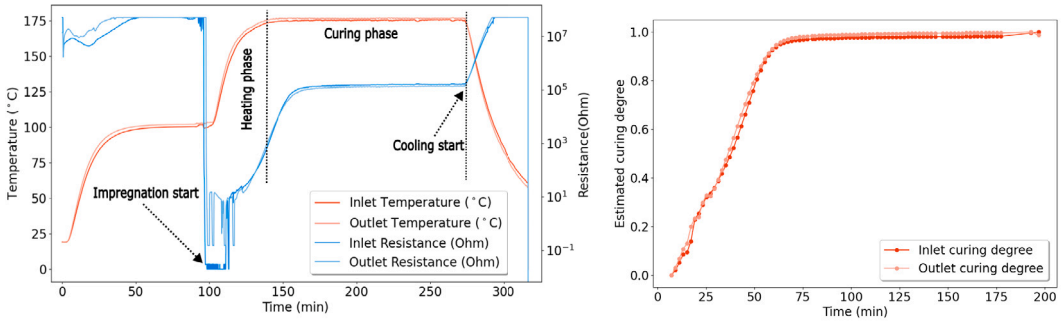

(a) (b)

Fig. 3. (a) Resistance and temperature measurements via a Synthesites disposable sensor during LRI process. (b) Curing degree estimation from dielectric sensor resistance data after applying temperature compensation.

MΩ, indicating successful impregnation. During the subsequent heating and curing stages, resistance variations qualitatively reflect key transitions: a decrease marks the point of minimum viscosity, followed by an increase indicating the onset of cross-linking. Final stabilization of the signal is commonly used by experts as an empirical indicator that the resin has reached a sufficient cure level for demolding.

In addition to resistance measurements, the sensor simultaneously monitors temperature, which is a critical parameter in non-isothermal curing cycle studies. Although resistance provides reliable qualitative information about the cure state, its interpretation under non-isothermal conditions becomes challenging due to the temperature-dependent nature of the resin's electrical properties [28]. Consequently, a compensation technique was implemented in this work to isolate curing effects from thermal influences, enabling accurate cure monitoring. As detailed in Appendix, the developed compensation method yields the cure degree estimates shown in Fig. 3(b), which served as ground truth for hyperspectral data regression model training and validation.

2.3. Hyperspectral imaging system

During the curing phase, the HSI system captured images from above, as illustrated in Fig. 1. Two broadband halogen lamps, positioned symmetrically at oblique angles, illuminated the sample. The HSI setup includes the *Specim FX17e* near-infrared hyperspectral camera which was employed to inspect the object under study in reflectance mode. The camera operates in the NIR range (935–1720 nm) with 224 spectral bands, a spatial resolution of 640 pixels, and a 38° field of view (FOV) lens. Following the push-broom principle, it captures one spatial line per frame, therefore to image the entire sample, either the camera or the object must be moved perpendicular to the scan line at a constant speed synchronized with the frame rate and field of view.

To convert the raw hyperspectral data into reflectance spectra, a radiometric calibration was performed. Before each acquisition, a white reference (99% Spectralon target) was measured under the same illumination conditions to account for the background response, while a dark reference (closed shutter) captured the sensor's noise offset. The reflectance of the sample was then calculated using Eq. (1), where $I_{\text{sample}}(\lambda, x)$ is the raw intensity measured from the sample at wavelength λ and spatial position x, $I_{\text{white}}(\lambda)$ is the intensity measured from the white reference (Spectralon target), and $I_{\text{dark}}(\lambda)$ is the dark signal acquired with the shutter closed. This calibration corrects detector responses and normalizes reflectance to a 0%–100% (0–1) range across all wavelengths, producing reliable spectral data [20].

$$R(\lambda, x) = \frac{I_{\text{sample}}(\lambda, x) - I_{\text{dark}}(\lambda)}{I_{\text{white}}(\lambda) - I_{\text{dark}}(\lambda)} \tag{1}$$

2.4. Data acquisition methodology

The LRI process involves stacking multiple material layers (Fig. 1). Each constituent material contributes distinct spectral features that may influence the predictive model. To characterize these individual contributions and assess their impact on the overall spectral signature, hyperspectral images of each component were first acquired separately using the HSI system before capturing the full setup.

A sample of each material was analysed using the *Specim LabScanner* system. This system consists of a conveyor belt that moves samples beneath a stationary camera. Key acquisition parameters included a camera-to-sample distance of 330 mm, an acquisition rate of 50 fps, and a scanning speed of 11.7 mm/s.

For in-process hyperspectral monitoring of large-scale composite parts manufactured via LRI, robotic integration of the imaging system

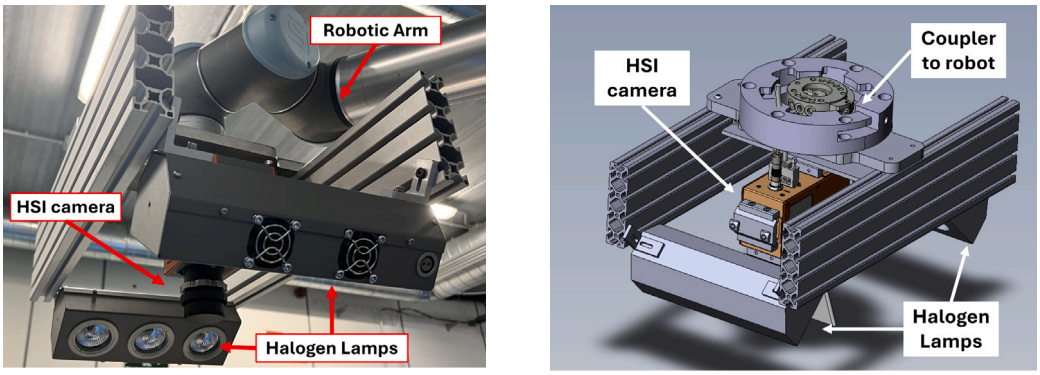

(a) (b)

Fig. 4. (a) FX17e hyperspectral camera and illumination system mounted on the Omron TM12 robotic arm. (b) CAD model of the coupling mount designed to attach the hyperspectral imaging system to the robotic arm.

is required. The entire hyperspectral system was mounted on a 6-axis Omron TM12 robotic arm (Fig. 4(a)) using a custom coupling mount (Fig. 4(b)). This setup is also well-suited for monitoring more complex parts due to the flexibility provided by the robotic arm in terms of trajectory control.

Camera parameters were carefully tuned to ensure complete and geometrically accurate capture of the entire 280 × 200 mm preform. The camera's working distance was set to 360 mm, yielding a 250 mm FOV in the cross-track (line) direction. With an acquisition rate of 50 fps, the robotic arm's scanning speed was set to 19.53 mm/s in the along-track (motion) direction. This configuration ensured a matched spatial resolution of around 0.4 mm/pixel in both cross-track and along-track directions, preserving geometric fidelity in the resulting hyperspectral data cube. Camera exposure time was set to 4 ms.

In total, two composite samples were monitored in this study. Hyperspectral images were acquired throughout the entire heating and curing phases, starting immediately after resin impregnation, with an acquisition interval of 2 min. For the first sample (Sample A), the complete LRI process was conducted under standard conditions, allowing the curing cycle to finish normally and dielectric sensor data was captured (Fig. 3(a)). In contrast, for the second sample (Sample B), the curing process was interrupted before completion, and dielectric sensor data was not acquired.

2.5. Hyperspectral image analysis

The acquired hyperspectral images require preprocessing before any further analysis to correct for undesirable phenomena arising from the measurement. Typically, both spatial and spectral preprocessing are applied to hyperspectral data [29]. In this study, spatial preprocessing is performed by defining Regions of Interest (ROIs) within the hyperspectral images. This isolates relevant data and reduces the size of the resulting hypercube, thereby lowering computational load and simplifying data management. The ROIs were defined based on the position of the dielectric sensors, which provide reference measurements of the curing degree, as described in Section 2.2. The data from these ROIs was then used for subsequent modelling using regression techniques.

Additionally, to ensure that the ROI defined in each acquisition corresponds to the same spatial area across different time points, a feature-based matching algorithm was implemented using the Oriented FAST and Rotated BRIEF (ORB) algorithm [30]. This approach allows for consistent ROI placement even in the presence of slight misalignments between acquisitions due to the lack of synchronization between robot movement start and camera acquisition start. Fig. 5 illustrates the selected ROIs (40 × 40 pixels) overlaid on the hyperspectral images (false RGB representation) at two different acquisition times. The red and blue marked ROIs indicate the spatial regions where the dielectric sensors are positioned (shown in Fig. 2(b), red inlet sensor and blue outlet sensor), ensuring that spectral information is consistently extracted from the same physical location throughout the curing process.

Spectral preprocessing was then applied to minimize variability unrelated to the target object, such as sensor noise or light scattering, which is especially prevalent in Near Infrared hyperspectral imaging (e.g., baseline shifts and non-linearities) [20]. In this study, the Standard Normal Variate (SNV) method was applied to mitigate the effects of light scattering present in the NIR spectra. The SNV method normalizes each pixel's spectral vector by subtracting its mean and dividing by its standard deviation. This standardization is applied independently to each pixel across all spectral bands, ensuring zero mean and unit variance per spectrum.

To study the correlation between spectral data and the curing degree of the inspected sample (Sample A), regression models were employed, specifically, Partial Least Squares Regression (PLS-R) and Support Vector Regression (SVR). These methods have previously been applied to regression problems involving NIR hyperspectral imaging data [31–33]. Both aim to predict the relationship between spectral data (input) and curing degree (output). PLS-R [34] identifies latent variables that capture key information from spectral predictors while maximizing correlation with the response variable. This makes it well-suited for collinear and high-dimensional data. In contrast, SVR [35,36] is a kernel-based method that maps input features into a higher-dimensional space, allowing it to model complex nonlinear relationships between spectral data and curing degree.

For regression model training, hyperspectral data from both ROIs (shown in Fig. 5) were used as input. The target output was the curing degree, inferred from dielectric sensor measurements taken at the same locations as the ROIs. For PLS-R, the optimal number of components was selected using cross-validation, minimizing the Mean Squared Error (MSE) instead of maximizing the coefficient of determination (R^2), to reduce overfitting and facilitate generalization. Similarly, SVR was trained on the same dataset, with hyperparameters optimized via grid search and 5-fold cross-validation to balance model complexity and accuracy. In both PLS-R and SVR, an initial regression model was trained using all hyperspectral image bands, excluding those at the spectral range boundaries to reduce noise from the camera's lower sensitivity at the edges.

In addition, feature selection techniques were applied to identify the most informative wavelengths for predicting curing degree. These included both model-specific and model-independent methods. For PLS-R, Variable Importance in Projection (VIP) scores from the initial model were used to select the top 20% of wavelengths contributing most to variance explanation. Two model-independent techniques were also used. Mutual Information (MI) [37,38] measured dependency between individual wavelengths and the curing degree, capturing both

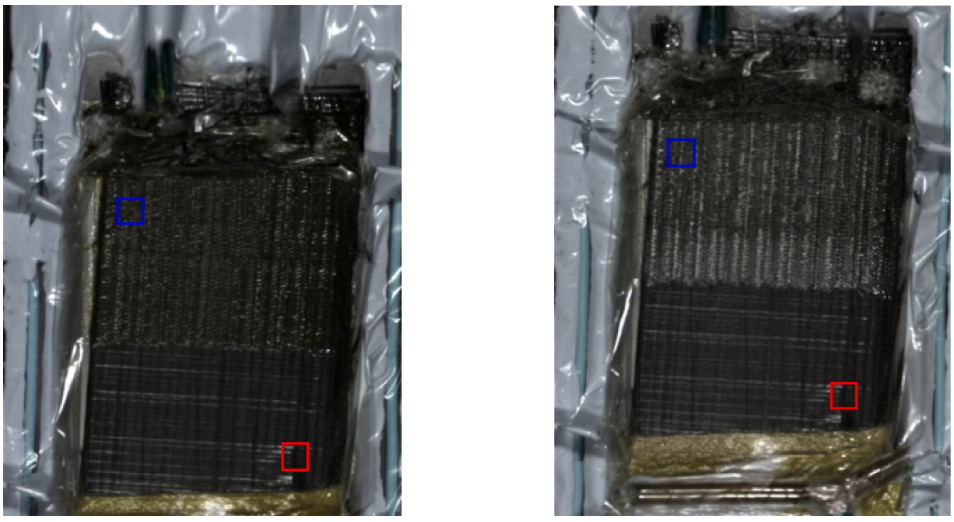

Fig. 5. Comparison of selected ROIs across different acquisition times. The red-marked ROIs indicate the spatial regions corresponding to the placement of the dielectric sensors, ensuring consistent spectral data extraction throughout the curing process. Feature-based matching using the ORB algorithm was applied to maintain spatial alignment between acquisitions.

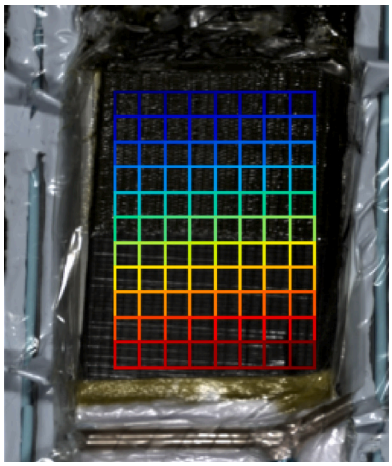

Fig. 6. Grid of ROIs defined on the HSI acquisition of the entire composite part for model prediction.

linear and nonlinear associations. Random Forest Regression (RF) [39] ranked features based on their contribution to reducing prediction error across an ensemble of decision trees. In total, four PLS-R models and three SVR models were trained: one using the full spectral dataset and the others using the selected wavelength subsets obtained through the described feature selection techniques. In all cases, the dataset was split into 80% for training and 20% for validation to evaluate model performance.

Finally, the best-performing model was used to predict the curing degree across a distributed grid of ROIs (Fig. 6) covering the entire sample surface. This enabled the generation of spatially resolved curing maps, allowing for a more comprehensive evaluation of curing uniformity across the entire composite part.

3. Results

3.1. Spectral characterization of RTM6-2 epoxy resin and other constituent materials of the LRI process

RTM6-2 is a pre-mixed tetra-functional epoxy-amine system. During the curing phase, a cross-linking reaction occurs between the oxirane rings of the epoxy monomers and the amine groups of the hardener [40]. The epoxy group undergoes oxirane ring-opening reactions during this process, initially reacting with primary amines to form secondary amines. These secondary amines subsequently react with additional epoxy groups to produce tertiary amines. This sequence of reactions leads to a reduction in the concentration of oxirane rings and amine groups, accompanied by an increase in the concentration of hydroxyl groups. These chemical transformations induce modifications in the molecular vibrational modes associated with key functional groups, affecting the way the material absorbs light in the near-infrared (NIR) spectrum.

Fig. 7 shows the reflectance spectra of the RTM6-2 epoxy resin acquired during its curing process. A clear evolution in the spectral signatures is observed as the curing process progresses over time, indicating chemical and physical changes in the resin system. Several absorption bands in the NIR spectrum enable the identification of functional groups of interest, as reported in the literature [19], and the evolution of the absorption bands associated with each reactive functional group over the cure reaction time might enable the monitoring of the reaction progress.

In the initial reaction stage (blue spectra), peaks observed between 1600 to 1700 nm are attributed to CH_3, CH_2 and CH groups. In particular, the peak at ≈1650 nm is related to the 1st overtone of the fundamental CH stretching vibration of the terminal epoxide ring and the peak at 1700 nm is assigned to the 1st overtone of the fundamental CH_2 and CH_3 stretching vibration mode [19]. A prominent peak is observed at approximately 1499 nm, associated with the combined absorption of primary and secondary amines. The literature attributes this peak to the combination of the fundamental NH_2 asymmetric and symmetric stretching vibrations. For kinetic studies, this peak offers valuable insights during the final stages of the reaction, when primary amine groups begin to disappear, and only secondary amine-epoxy reactions remain active [41].

The hydroxyl group is primarily reflected in Fig. 7 between 1428 and 1437 nm, which is attributed to the first overtone of the OH stretching vibrations [42]. Hydroxyl groups are useful for monitoring the curing reaction, as their appearance indicates that the reaction is taking place. However, the authors of [41] caution against relying solely on this peak for such purposes, as hydroxyl groups form hydrogen bonds with each other or with other system components. This results in a baseline shift at the lower wavenumber tail of the peak due to hydrogen bonding.

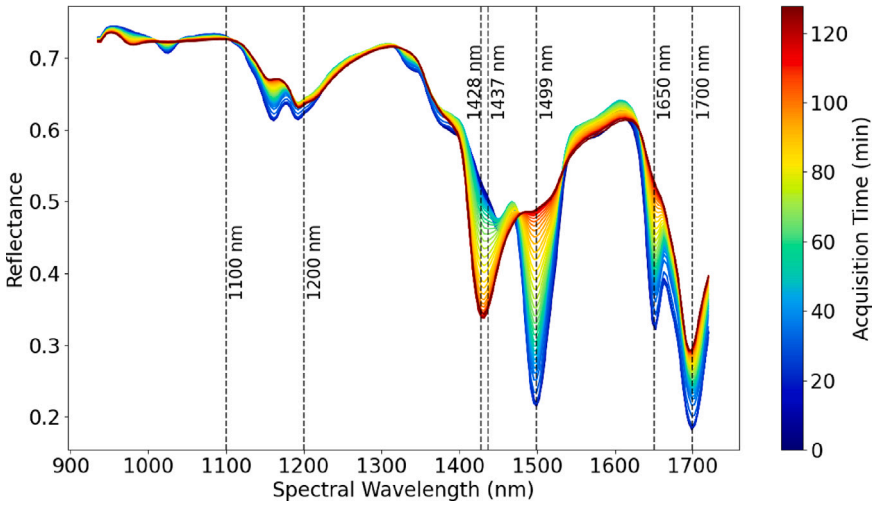

Fig. 7. Temporal evolution of RTM6-2 resin spectra acquired during curing process, along with key wavelengths reported in the literature.

And finally, at the beginning of the spectrum, a weak combination of peaks can be visualized in the range of 1100 to 1200 nm, attributed to the absorption bands of various CH groups [43].

As the monitored process is non-isothermal, it is essential to consider the potential influence of temperature on the acquired NIR spectra, as both peak position shifts and intensity changes may occur with temperature variations [44]. Temperature-induced intensity variations in vibrational spectroscopy have been reported for epoxy resins, where increased temperature leads to reduced absorption peak intensities. These intensity changes are fully reversible upon cooling, suggesting they are primarily related to physical property variations, such as changes in density or viscosity, rather than permanent chemical transformations [45]. In addition, such intensity variations generally manifest as baseline offsets or global intensity changes, rather than as distinct spectral features associated with specific chemical groups. These effects are analogous to scattering-induced additive baseline shifts and multiplicative scaling commonly observed in NIR hyperspectral imaging and can be mitigated using appropriate spectral preprocessing technique like SNV as commented in Section 2.5. In contrast, peak shifts induced by temperature are generally small, typically below 1–2 nm, and often fall below the spectral resolution of the acquisition system, including the HSI equipment used in this study [46,47].

Despite the spectral reflectance of the resin evolves throughout the curing process, with notable variations occurring in mentioned absorption bands, this study focuses on assessing the feasibility of HSI for monitoring the resin curing process within an LRI setup, where multiple materials coexist. During LRI, various materials are present, and their spectral signatures may interfere with the resin's spectral signature. For this reason, the characteristic spectrum of each of the basic constituents involved in the process was measured, including carbon fibre, the polymer vacuum bag and the polymer flow media. The raw reflectance spectra of the mentioned materials are shown in Fig. 8.

The reflectance spectra of the materials reveal important characteristics that will influence in-situ spectral monitoring. As expected, the carbon fibre exhibits a nearly flat spectrum with reflectance values close to zero across the entire measured wavelength range, consistent with the behaviour of highly absorptive black materials.

During the infusion process, the resin impregnates the carbon fibres and a thin superficial layer on top of them is formed. Since the incident light cannot penetrate deeper fibre layers, the measured spectral signal is attenuated compared to bulk resin due to this limited sampling volume, reducing the signal-to-noise ratio.

The vacuum bag and flow media were characterized by placing them over a highly reflective white background. On this setup, the signal of both materials exhibit relatively high reflectance values due to their low thickness, and although they attenuate the overall signal, neither shows significant absorption features in the wavelength regions where the resin displays spectral changes during curing (e.g., 1428, nm and 1499, nm). Therefore, although these materials reduce the absolute reflectance signal and are expected to distort the spectra obtained during LRI monitoring compared to those of the RTM6-2 resin bulk sample (Fig. 7), certain spectral differences related to resin curing should still be observable.

3.2. LRI curing phase monitoring using hyperspectral imaging

Fig. 9 presents the complete temporal evolutions of the mean SNV-normalized spectra of the upper-left (Fig. 9(a)) and lower-right (Fig. 9(b)) ROIs shown in Fig. 5 of Sample A. Spectral differences are observed when comparing the data from the ROIs, confirming that the presence of additional materials influences the resulting spectra. In this case, the only distinction is the presence of a flow media in the upper region, whereas the lower region lacks it. When comparing these spectra with the resin spectra shown in Fig. 7, noticeable differences also emerge across multiple absorption bands, likely attributed to the influence of additional materials present in the LRI setup explained in Section 3.1. Despite this variations, several key spectral features exhibit trends consistent with those observed in resin, reinforcing their potential relevance for tracking the curing process. In particular, the key absorption features at 1428 nm and 1499 nm exhibit a consistent temporal evolution, suggesting that these spectral features may be reliable indicators of curing progression despite the presence of additional materials.

To assess the effectiveness of the proposed approach, the regression models introduced in Section 2.5 were evaluated using the hyperspectral reflectance data collected from the two ROIs of Sample A and the corresponding inferred curing degree values obtained from dielectric sensors (Fig. 2(b)). The performance of the trained regression models was evaluated based on the coefficient of determination (R^2), the root mean squared error (MSE) and the mean absolute error (MAE) on the validation set (Table 1). Also, Fig. 10 presents and compares the results for the different feature selection approaches, showing a strong correlation between the different methods, with slight variations depending on the selection criteria. Notably, the chosen wavelengths correspond to spectral regions exhibiting significant reflectance changes during the curing process (Fig. 9). Specifically, peaks observed around 1428 and 1499 nm align well with selected features, reinforcing their importance in tracking chemical transformations.

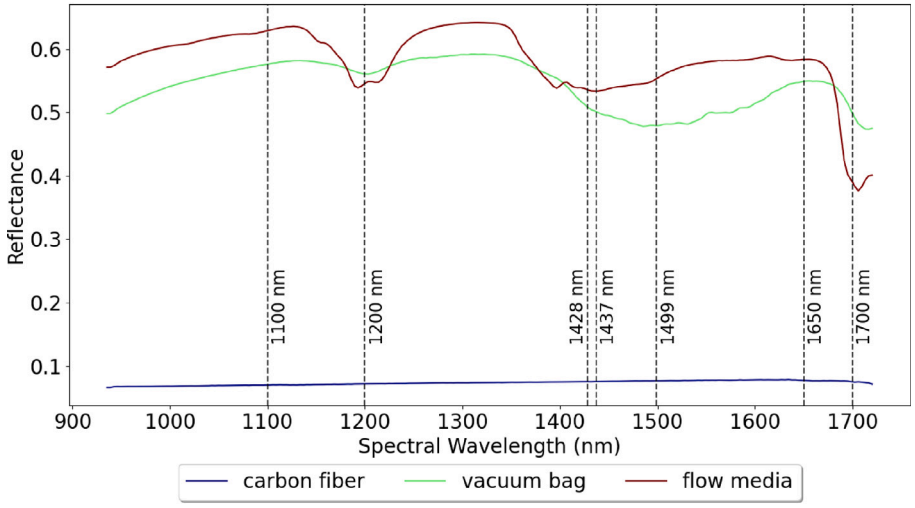

Fig. 8. Spectral signature of the materials involved in the LRI process.

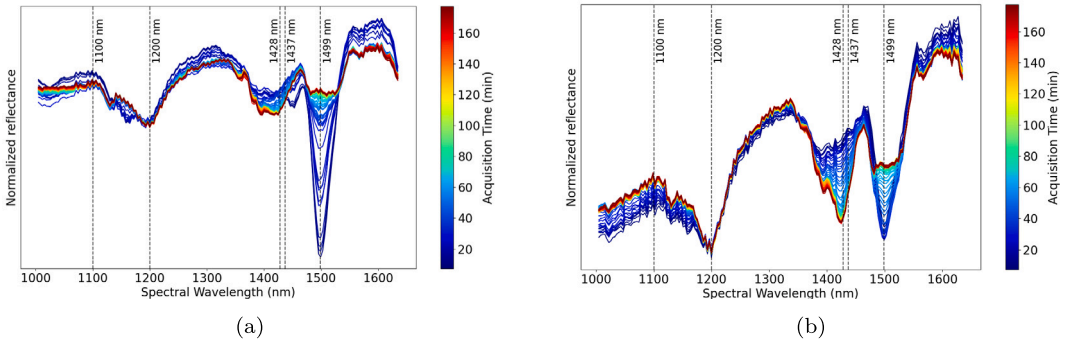

Fig. 9. SNV-normalized spectra of Sample A. (a) Upper-left ROI (b) Lower-right ROI.

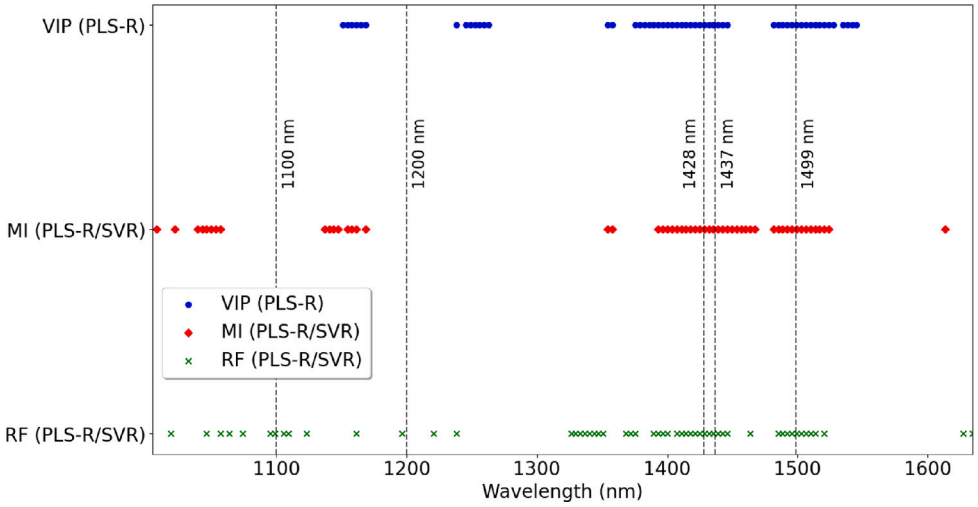

Fig. 10. Wavelength selection results by different feature selection techniques.

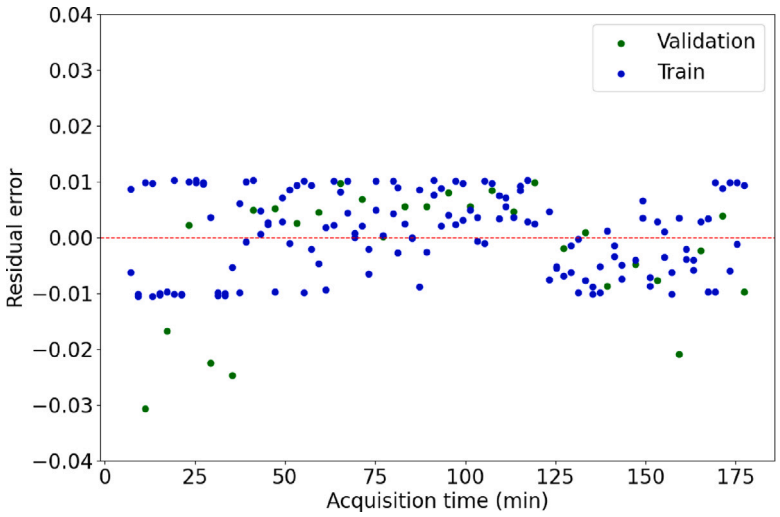

Fig. 11. Residual plot of SVR model trained with all features.

Table 1
Regression performance metrics for PLS-R and SVR models on the validation set.

Model	R^2	RMSE	MAE
PLS (All Features)	0.9439	0.0661	0.0507
PLS (VIP)	0.9498	0.0625	0.0561
PLS (MI)	0.9711	0.0474	0.0368
PLS (RF)	0.9620	0.0544	0.0445
SVR (All Features)	**0.9983**	**0.0114**	**0.0086**
SVR (MI)	0.9818	0.0376	0.0188
SVR (RF)	0.9745	0.0445	0.0210

All models demonstrate strong predictive capability, with high R^2 values and low RMSE and MAE. Among them, the SVR model trained on all spectral features achieves the best overall performance ($R^2 = 0.9983$, RMSE = 0.0114, MAE = 0.0086). The residual plot in Fig. 11 provides further insights into the predictive capability of this model. The PLS-R models also perform well, although their performance is more dependent on feature selection. In particular, feature selection using Mutual Information (MI) and Random Forest (RF) contributed to improved generalization of the PLS-R model Conversely, for SVR, feature selection slightly reduces performance, suggesting that the model benefits more from the full spectral range. Overall, these results highlight that while both modelling approaches are effective, SVR achieves superior accuracy, and PLS-R is more sensitive to the choice of input features.

The best-performing model is then used to predict the curing state across the entire sample, using the grid of ROIs shown in Fig. 6. The predicted curing degree, a continuous value between 0 (uncured) and 1 (fully cured) and output by the best-performing regression model, was discretized into 20 levels with increments of 0.05 (i.e., 5%) to generate spatially resolved curing heatmaps, as shown in Fig. 12. Overall, all defined ROIs exhibit consistent trends, with no significant outliers observed.

Furthermore, the same prediction process was applied to Sample B data to generate curing maps (Fig. 13) and qualitatively assess the generalization capability of the trained models. As observed with Sample A, the progression of the curing state across different ROIs in Sample B follows a consistent spatial trend. However, the predicted curing degree does not reach the same levels as in Sample A over equivalent curing durations, and some spatial inhomogeneities are observed. These differences can be attributed to the temperature distribution during the process. As shown in Fig. 14, Sample A exhibits a uniform and higher temperature profile at both inlet and outlet sensors. In contrast, Sample B displays a slower and uneven temperature ramp, particularly at the outlet. These temperature differences and spatial inhomogeneities could explain the curing level discrepancies seen across samples and within Sample B itself.

4. Conclusions

This study demonstrates the feasibility of using Near-Infrared Hyperspectral Imaging (NIR-HSI) for monitoring of the curing degree in Liquid Resin Infusion (LRI) manufacturing. By establishing a correlation between hyperspectral reflectance data and curing degree measurements using a dielectric sensor, the results highlight the potential of NIR-HSI as a non-invasive alternative for in-line quality control of composite manufacturing processes.

The findings contribute to the development of non-destructive monitoring techniques, particularly for high-value sectors such as aerospace and automotive industries, where precise manufacturing processes are essential. The ability to track resin polymerization through hyperspectral imaging provides a significant advantage in ensuring production consistency and material performance. The study successfully demonstrates the efficacy of NIR-HSI in monitoring the curing process by correlating changes in hyperspectral reflectance with key chemical transformations occurring during polymerization. Specifically, variations in reflectance at chemically relevant wavelengths correspond to changes in functional groups involved in curing reactions, confirming the ability of hyperspectral imaging to provide real-time insights into resin polymerization. The use of regression models further validates the relationship between hyperspectral data and the actual curing degree, reinforcing NIR-HSI as a promising tool for in-line quality assessment in composite manufacturing.

Compared to conventional dielectric sensors, NIR-HSI offers several advantages. It is a fully non-contact, non-destructive method with real-time monitoring capabilities, eliminating the need for embedded sensors that could alter material properties or require additional processing steps. Furthermore, NIR-HSI provides both spatial and spectral information, enabling the monitoring of curing heterogeneity across the entire sample rather than at discrete sensor locations. This spatial awareness is particularly valuable in composite manufacturing, where variations in resin flow and polymerization kinetics can significantly affect final material properties.

Overall, the results emphasize the potential of NIR-HSI as an effective and scalable technology for non-invasive monitoring in composite manufacturing. Further work will focus on improving and validating these findings with additional real-world data and on intentionally inducing curing inhomogeneities to assess the system's ability to generate accurate curing maps, one of its main advantages for detecting spatial variability in the curing process, a key parameter in composite manufacturing.

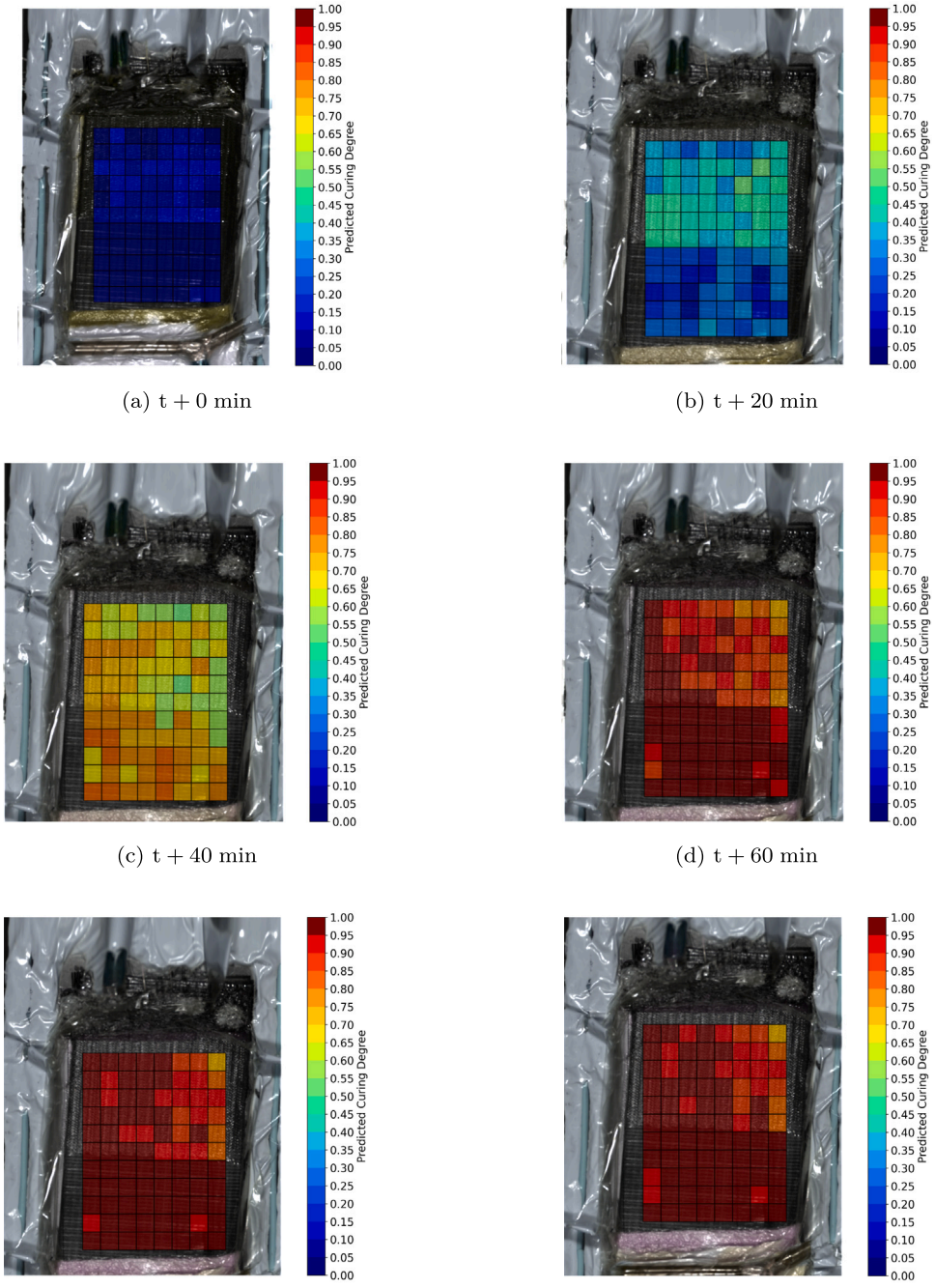

(a) t + 0 min (b) t + 20 min

(c) t + 40 min (d) t + 60 min

(e) t + 80 min (f) t + 100 min

Fig. 12. Predicted curing degree maps for Sample A at different acquisition times (t) after resin impregnation, generated using the SVR-All model. The continuous model output (curing degree between 0 and 1) was discretized into 20 levels (5% intervals) to visualize spatial variations in the degree of cure across the sample surface.

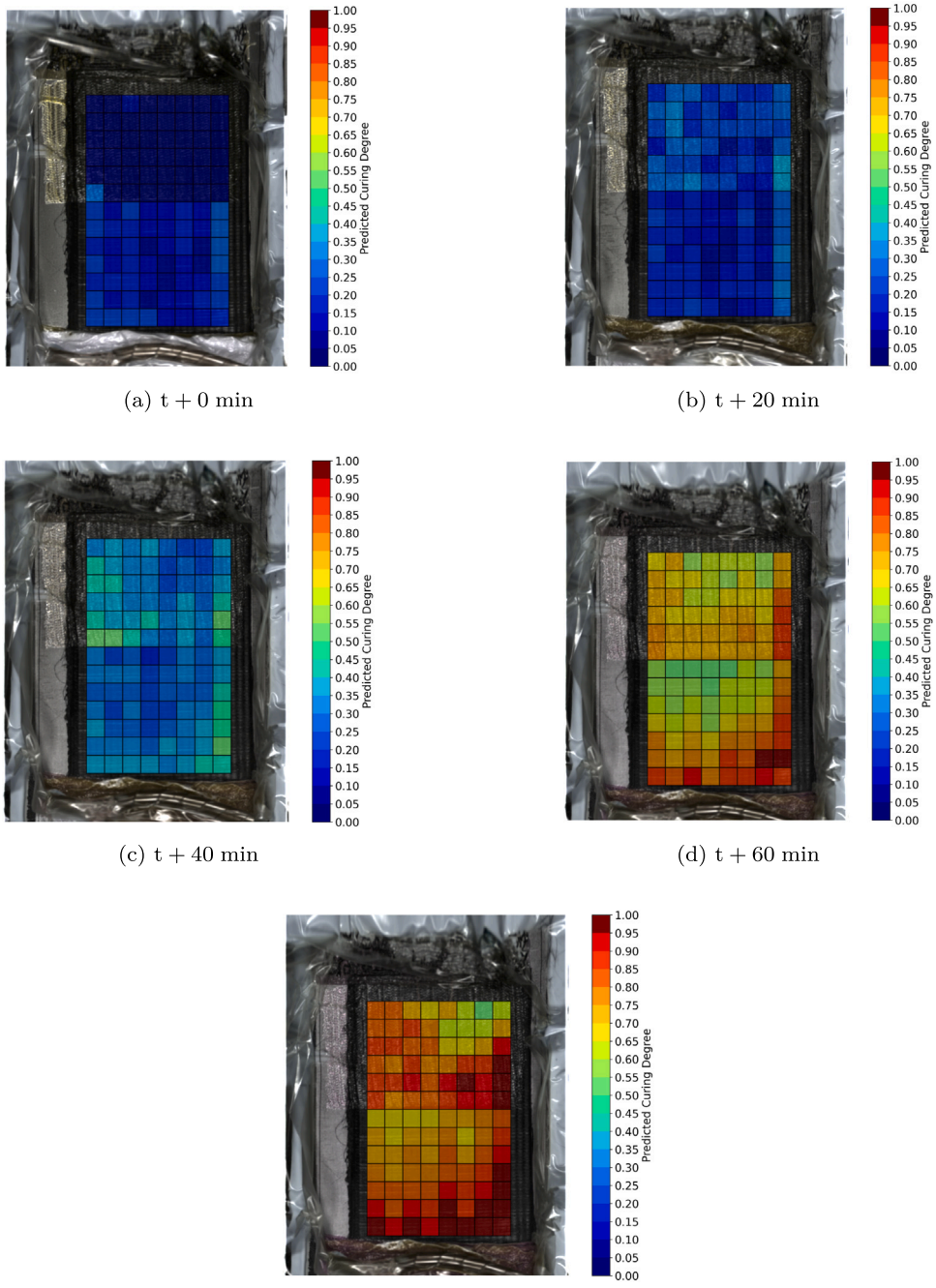

(a) t + 0 min (b) t + 20 min

(c) t + 40 min (d) t + 60 min

(e) t + 70 min

Fig. 13. Predicted curing degree maps for Sample B at different acquisition times (t) after resin impregnation, generated using the SVR-All model. The continuous model output (curing degree between 0 and 1) was discretized into 20 levels (5% intervals) to visualize spatial variations in the degree of cure across the sample surface.

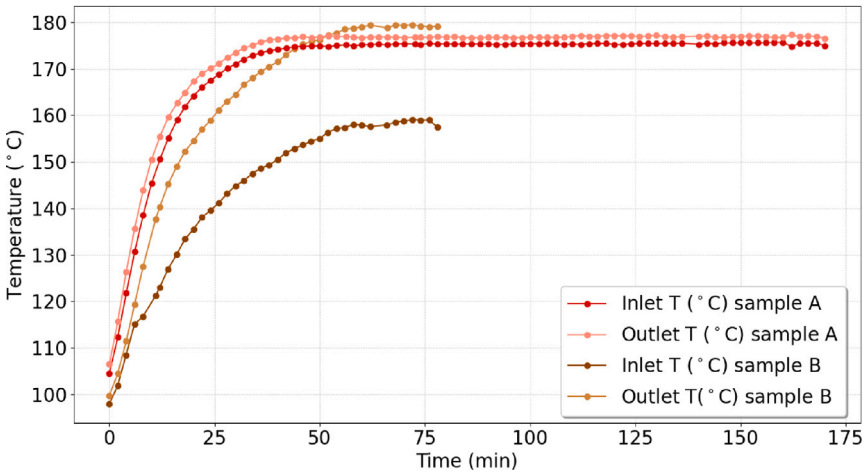

Fig. 14. Temperature measurements recorded during the LRI curing process for both Sample A and Sample B, showing inlet and outlet sensor data over time.

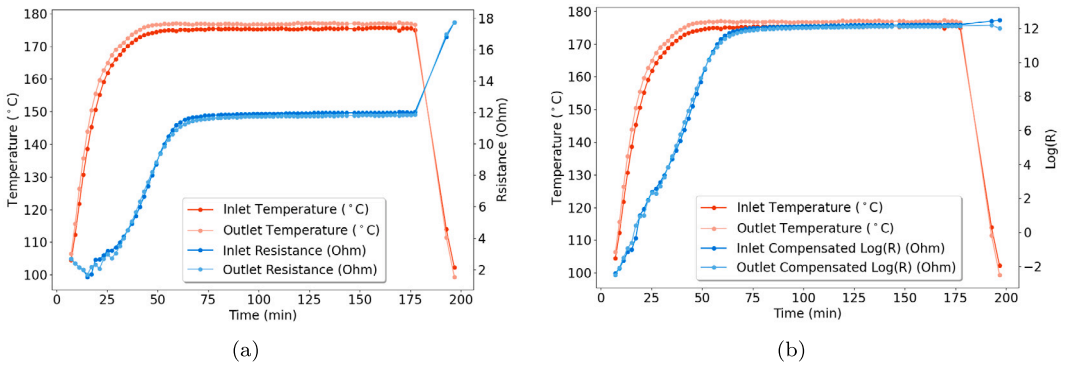

Fig. A.15. Temperature and resistance values measured by the sensor during HSI acquisition in the LRI process. Dots indicate HSI acquisition times. (a) Raw temperature and resistance data. (b) Raw temperature and temperature-compensated resistance.

CRediT authorship contribution statement

Xabier Zurutuza Lasa: Conceptualization, Methodology, Software, Formal analysis, Writing – original draft. **Laura Arévalo Díaz:** Conceptualization, Methodology, Formal analysis, Writing – review & editing. **Janusz Poplawski:** Project administration, Conceptualization, Methodology, Software, Formal analysis, Writing – review & editing. **Cristian Builes Cárdenas:** Resources, Data collection, Writing – review & editing. **Tania Grandal González:** Resources, Data collection, Writing – review & editing. **Arantzazu Núñez Cascajero:** Resources, Data collection. **Rubén Ruiz Lombera:** Resources, Data collection. **Paula Rodriguez Alonso:** Resources, Data collection. **Mario Román Rodríguez:** Resources, Data collection. **Daniel Maestro-Watson:** Conceptualization, Methodology, Formal analysis, Writing – review & editing. **Luka Eciolaza Echeverria:** Conceptualization, Methodology, Formal analysis, Writing review & editing.

Funding

This study was conducted within the framework of the FLASH-COMP project (Flawless and Sustainable Production of Composite Parts through a Human-Centred Digital Approach), which receives funding from the European Union's Horizon Europe research and innovation programme under grant agreement No. 101058458.

Declaration of competing interest

The authors declare the following financial interests/personal relationships which may be considered as potential competing interests: Xabier Zurutuza Lasa reports financial support was provided by Horizon Europe. If there are other authors, they declare that they have no known competing financial interests or personal relationships that could have appeared to influence the work reported in this paper.

Appendix. Curing degree calculation from dielectric sensor data

The disposable sensor from Synthesites [26] provides temperature and resistance information at the inspected point. In Section 2.2, it is mentioned that resistance values serve as a reliable marker for the state of curing of the sample. However, in non-isothermal curing cycles, this electrical property must be compensated due to the influence of temperature on electrical properties, and consequently, on the resistance values measured by the sensor [28].

Fig. 3(a) shows the complete dataset acquired by the sensor, capturing all phases of the LRI process. After the curing stage, temperature decreases, while resistance increases linearly. Since resistance is considered an indicator of the curing degree, it should remain nearly constant during this phase. Therefore, we use these data to develop a linear model to compensate resistance based on temperature variations. Notably, the resistance axis is logarithmic, meaning we aim to establish a linear relationship between log(resistance) and temperature in the post-curing stage. The compensation function is defined as:

$$\log(\rho_{\text{comp}}) = \log(\rho) - k(T - T_0)$$

where $\log(\rho_{\text{comp}})$ is the compensated logarithmic resistance, $\log(\rho)$ is the measured logarithmic resistance, T represents the temperature, T_0 is a reference temperature, and k is the compensation coefficient, derived from the linear relationship observed in the data. Applying this function

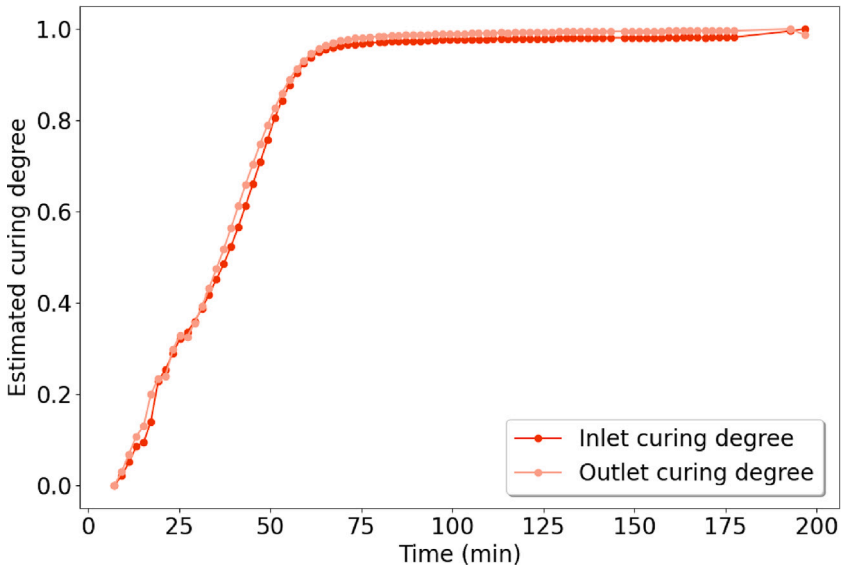

Fig. A.16. Resistance and temperature data measured by the Synthesites disposable sensor during the manufacturing of the composite part using the LRI process.

allows us to adjust log(resistivity) values to account for temperature variations (Fig. A.15).

Using the compensated log(resistivity), we infer the curing degree of the composite part at both dielectric sensor locations. We assume that the normalized compensated log(resistivity) values (scaled between 0 and 1) directly represent the curing degree (see Fig. A.16).

Data availability

The dataset used in this study is publicly available on Zenodo at the following DOI: https://doi.org/10.5281/zenodo.15087655.

References

[1] D. Hull, T.W. Clyne, An introduction to composite materials, 1996, http://dx.doi.org/10.1017/CBO9781139170130.
[2] P. Mallick, Fiber-reinforced composites: Materials, manufacturing, and design, third edition, 2007.
[3] M.O. Seydibeyoğlu, A.K. Mohanty, M. Manjusri, Fiber technology for fiber-reinforced composites, 2017, http://dx.doi.org/10.1016/C2015-0-05497-1.
[4] J. Zhang, G. Lin, U. Vaidya, H. Wang, Past, present and future prospective of global carbon fibre composite developments and applications, Compos. Part B: Eng. 250 (2023) 110463.
[5] Q. Govignon, S. Bickerton, P. Kelly, 6 - liquid composite molding processes, in: Advanced Fiber-Reinforced Polymer(FRP) Composites for Structural Applications, second ed., 2023, pp. 101–136, http://dx.doi.org/10.1016/B978-0-12-820346-0.00006-X.
[6] A. Hindersmann, Confusion about infusion: An overview of infusion processes, Compos. Part A: Appl. Sci. Manuf. 126 (2019) 105583, http://dx.doi.org/10.1016/j.compositesa.2019.105583.
[7] C. Sacco, A.B. Radwan, A. Anderson, R. Harik, E. Gregory, Machine learning in composites manufacturing: A case study of automated fiber placement inspection, Compos. Struct. 250 (2020) 112514.
[8] R. Schmitt, T. Pfeifer, C. Mersmann, A. Orth, A method for the automated positioning and alignment of fibre-reinforced plastic structures based on machine vision, CIRP Ann 57 (2008) 501–504.
[9] V.R. Marrazzo, A. Laudati, M. Vitale, F. Fienga, G. Iagulli, M. Raffone, A. Cusano, M. Giordano, A. Cutolo, G. Breglio, Liquid resin infusion process validation through fiber optic sensor technology, Sensors (Basel, Switz.) 22 (2022) 508, http://dx.doi.org/10.3390/s22020508.
[10] R. Stanik, A. Langkamp, M. Müller, M. Gude, A. Boczkowska, Experimental investigation of the curing behaviour of fibre composite structures with snap-cure polymer systems, Int. J. Struct. Integr. 9 (2018) 768–778, http://dx.doi.org/10.1108/IJSI-12-2017-0070.
[11] Y.A. Tajima, Monitoring cure viscosity of epoxy composite, Polym. Compos. 3 (1982) 162–169, http://dx.doi.org/10.1002/pc.750030310.
[12] J.-S. Kim, D.G. Lee, On-line cure monitoring and viscosity measurement of carbon fiber epoxy composite materials, J. Mater. Process. Technol. 37 (1993) 405–416, http://dx.doi.org/10.1016/0924-0136(93)90105-F.
[13] S.D. Schwab, R.L. Levy, G.G. Glover, Sensor system for monitoring impregnation and cure during resin transfer molding, Polym. Compos. 17 (1996) 312–316, http://dx.doi.org/10.1002/pc.10616.
[14] A. Kyriazis, C. Pommer, D. Lohuis, K. Rager, A. Dietzel, M. Sinapius, Comparison of different cure monitoring techniques, Sensors 22 (2022) 7301, http://dx.doi.org/10.3390/s22197301.
[15] M. Sabu, E. Bementa, Y. Jaya Vinse Ruban, S. Ginil Mon, A novel analysis of the dielectric properties of hybrid epoxy composites, Adv. Compos. Hybrid Mater. 3 (2020) 325–335.
[16] R. Montanini, L. d'Acquisto, Simultaneous measurement of temperature and strain in glass fiber/epoxy composites by embedded fiber optic sensors: I. Cure monitoring, Smart Mater. Struct. 16 (2007) 1718.
[17] A. Chaloupka, T. Pflock, R. Horny, N. Rudolph, S.R. Horn, Dielectric and rheological study of the molecular dynamics during the cure of an epoxy resin, J. Polym. Sci. Part B: Polym. Phys. 56 (2018) 907–913.
[18] M. Salzmann, W. Märzinger, M. Teuchtmann, B. Ravindran, U. Kirschnick, E. Fauster, Near-infrared spectroscopy in resin transfer molding—determination of the degree of cure, Int. J. Adv. Manuf. Technol. 132 (2024) 5557–5565, http://dx.doi.org/10.1007/s00170-024-13671-z.
[19] C. Billaud, M. Vandeuren, R. Legras, V. Carlier, Quantitative analysis of epoxy resin cure reaction: A study by near-infrared spectroscopy, Appl. Spectrosc. 56 (2002) 1413–1421, http://dx.doi.org/10.1366/00037020260377706.
[20] J.M. Amigo, Hyperspectral imaging, 2019, Vol. 32.
[21] L.M. Kandpal, E. Park, J. Tewari, B.-K. Cho, Spectroscopic techniques for non-destructive quality inspection of pharmaceutical products: A review, J. Biosyst. Eng. 40 (2015) 394–408, http://dx.doi.org/10.5307/JBE.2015.40.4.394.
[22] T. Nishii, K. Matsuzaki, S. Morita, Real-time determination and visualization of two independent quantities during a manufacturing process of pharmaceutical tablets by near-infrared hyperspectral imaging combined with multivariate analysis, Int. J. Pharm. 590 (2020) 119871, http://dx.doi.org/10.1016/j.ijpharm.2020.119871.
[23] J.M. Amigo, I. Martí, A. Gowen, Chapter 9 - hyperspectral imaging and chemometrics: A perfect combination for the analysis of food structure, composition and quality, in: Data Handling in Science and Technology, Vol. 28, 2013, pp. 343–370, http://dx.doi.org/10.1016/B978-0-444-59528-7.00009-0.
[24] D. Saha, A. Manickavasagan, Machine learning techniques for analysis of hyperspectral images to determine quality of food products: A review, Curr. Res. Food Sci. 4 (2021) 28–44, http://dx.doi.org/10.1016/j.crfs.2021.01.002.
[25] M. Salzmann, Y. Blößl, A. Todorovic, R. Schledjewski, Usage of near-infrared spectroscopy for inline monitoring the degree of curing in RTM processes, Polymers 13 (2021) 3145, http://dx.doi.org/10.3390/polym13183145.
[26] Aerospace - PRODUCTS - Sensors - Disposable Sensors.
[27] A. Torre-Poza, A.M.R. Pinto, T. Grandal, N. González-Castro, L. Carral, E. Rodríguez-Senín, Challenges of complex monitoring of the curing parameters in coupons for LRI manufacturing, INCAS Bull. 13 (1) (2021) 203–210, http://dx.doi.org/10.13111/2066-8201.2021.13.1.21.
[28] Aerospace - SOLUTIONS - Cure Monitoring of HexFlow® RTM6-1 -.
[29] M. Vidal, J.M. Amigo, Pre-processing of hyperspectral images. Essential steps before image analysis, Chemometr. Intell. Lab. Syst. 117 (2012) 138–148, http://dx.doi.org/10.1016/j.chemolab.2012.05.009.
[30] E. Rublee, V. Rabaud, K. Konolige, G. Bradski, ORB: An efficient alternative to SIFT or SURF, 2011.

[31] J.-H. Cheng, D.-W. Sun, Partial least squares regression (PLSR) applied to NIR and HSI spectral data modeling to predict chemical properties of Fish muscle, Food Eng. Rev. 9 (2017) 36–49, http://dx.doi.org/10.1007/s12393-016-9147-1.
[32] S. Hitchman, M. Loeffen, M. Reis, C. Craigie, Robustness of hyperspectral imaging and PLSR model predictions of intramuscular fat in Lamb M. Longissimus lumborum across several flocks and years, Meat Sci. 179 (2021) 108492, http://dx.doi.org/10.1016/j.meatsci.2021.108492.
[33] F. Tan, X. Mo, S. Ruan, T. Yan, P. Xing, P. Gao, W. Xu, W. Ye, Y. Li, X. Gao, T. Liu, Combining vis-NIR and NIR spectral imaging techniques with data fusion for rapid and nondestructive multi-quality detection of Cherry tomatoes, Foods 12 (2023) 3621, http://dx.doi.org/10.3390/foods12193621.
[34] H. Abdi, Partial least squares regression and projection on latent structure regression (PLS regression), WIREs Comput. Stat. 2 (2010) 97–106, http://dx.doi.org/10.1002/wics.51.
[35] C.-C. Chang, C.-J. Lin, LIBSVM: A library for support vector machines, ACM Trans. Intell. Syst. Technol. 2 (2011) 1–27, http://dx.doi.org/10.1145/1961189.1961199.
[36] A.J. Smola, B. Schölkopf, A tutorial on support vector regression, Stat. Comput. 14 (2004) 199–222, http://dx.doi.org/10.1023/B:STCO.0000035301.49549.88.
[37] H. Peng, F. Long, C. Ding, Feature selection based on mutual information criteria of max-dependency, max-relevance, and min-redundancy, IEEE Trans. Pattern Anal. Mach. Intell. 27 (2005) 1226–1238, http://dx.doi.org/10.1109/TPAMI.2005.159.
[38] X.-H. Ma, Z.-G. Chen, S. Liu, J.-M. Liu, X.-s. Tian, Wavelength selection method for near-infrared spectroscopy based on the combination of mutual information and genetic algorithm, Talanta 286 (2025) 127573, http://dx.doi.org/10.1016/j.talanta.2025.127573.
[39] L. Breiman, Random forests, Mach. Learn. 45 (2001) 5–32, http://dx.doi.org/10.1023/A:1010933404324.
[40] J. Moosburger-Will, M. Greisel, M.G. Sause, R. Horny, S. Horn, Influence of partial cross-linking degree on basic physical properties of RTM6 epoxy resin, J. Appl. Polym. Sci. 130 (2013) 4338–4346.
[41] J. Mijović, S. Andjelić, J.M. Kenny, In situ real-time monitoring of epoxy/amine kinetics by remote near infrared spectroscopy, Polym. Adv. Technol. 7 (1996) 1–16.
[42] Q.-F. Liu, D. Li, Y.-D. Zeng, W.-Z. Huang, Determination of gel time of prepreg in copper clad laminate industry by near infrared spectroscopy, J. Near Infrared Spect. 29 (2021) 5–10, http://dx.doi.org/10.1177/0967033520963799.
[43] M. Fischer, C.D. Tran, Evidence for kinetic inhomogeneity in the curing of epoxy using the near-infrared multispectral imaging technique, Anal. Chem. 71 (1999) 953–959, http://dx.doi.org/10.1021/ac981030b.
[44] M. Blanco, D. Valdés, Influence of temperature on the predictive ability of near infrared spectroscopy models, J. Near Infrared Spect. 12 (2004) 121–126, http://dx.doi.org/10.1255/jnirs.416.
[45] E. Duemichen, M. Javdanitehran, M. Erdmann, V. Trappe, H. Sturm, U. Braun, G. Ziegmann, Analyzing the network formation and curing kinetics of epoxy resins by in situ near-infrared measurements with variable heating rates, Thermochim. Acta 616 (2015) 49–60, http://dx.doi.org/10.1016/j.tca.2015.08.008.
[46] V.S. Langford, A.J. McKinley, T.I. Quickenden, Temperature dependence of the visible-near-infrared absorption spectrum of liquid water, J. Phys. Chem. A 105 (2001) 8916–8921, http://dx.doi.org/10.1021/jp010093m.
[47] J. Lin, C.W. Brown, Universal approach for determination of physical and chemical properties of water by near-IR spectroscopy, Appl. Spectrosc. 47 (1993) 1720–1727, http://dx.doi.org/10.1366/0003702934334589.